RSC Advances

PAPER

View Article Online
View Journal | View Issue

Check for updates

Cite this: *RSC Adv.*, 2021, **11**, 38849

Thermal degradation of defective high-surface-area UiO-66 in different gaseous environments†

Muhammad Athar,[ab] Przemyslaw Rzepka,[ab] Debora Thoeny,[b] Marco Ranocchiari *[a] and Jeroen Anton van Bokhoven *[ab]

Received 14th July 2021
Accepted 11th November 2021

DOI: 10.1039/d1ra05411b

rsc.li/rsc-advances

UiO-66 is a versatile zirconium-based MOF, which is thermally stable up to 500 °C. In the present work, the thermal degradation of UiO-66 with a high number of defects has been studied in inert, oxidative and reductive environments. A sample of UiO-66 with a high BET surface area of 1827 $m^2\ g^{-1}$ was prepared, which contains 2.3 missing linkers per hexa-zirconium node, as calculated by the thermogravimetric curve. The crystalline framework of this UiO-66 sample collapses at 250 °C, while thermal decomposition starts at 450 °C in the oxidative environment and at 500 °C in the reductive and inert environments. The BET surface area of the MOF is affected variably by heating under different gaseous conditions. Under inert conditions, porosity is maintained up to 711 $m^2\ g^{-1}$, which is quite high when compared to that under reductive (527 $m^2\ g^{-1}$) or oxidative (489 $m^2\ g^{-1}$) conditions. Upon complete thermal decomposition at 600 °C, the MOF produces predominantly tetragonal zirconia. TEM images of the thermally decomposed samples show that the shape of the original MOF crystal is maintained during the heating process in the inert and reductive environments, whereas under oxidative conditions, all of the carbon is burnt to carbon dioxide, leaving no carbon matrix as the support.

Introduction

Metal–organic frameworks (MOFs), crystalline materials made by the combination of organic linkers with inorganic units, are among the most compelling class of materials discovered in the past decades with potential applications in gas storage, separation and catalysis in gas and liquid media.[1,2] It is important to assess the stability of MOFs because it is directly related to their applicability in various liquid and gaseous environments.[3,4] Considerable effort has been made to find ways to stabilize MOFs depending on their use.[5] Framework modification, such as the introduction of stabilizing agents with ligands or metals into the framework, camouflages the active sites of the MOFs, thereby enhancing their stability.[6–9] It is essential to study the stability parameters and degradation mechanisms of MOFs in the media that are required for their application. Degradation of MOFs by liquids and gases has been studied.[10–13] The temperature-induced decomposition of a MOF may differ from its crystalline stability.[14] Some MOFs lose their crystalline structure upon heating, becoming amorphous over a wide temperature range before any actual thermal decomposition occurs.

MOFs are useful because of their high surface area. UiO-66 is a versatile zirconium-based MOF having a BET surface area of 1100–1200 $m^2\ g^{-1}$.[15] Its surface area can be enhanced by introducing defects into the framework, which may also improve the functionality of the material.[16,17] The "missing-linker" defect can be developed by adding a modulator (*e.g.*, a monocarboxylic acid) during synthesis, which then occupies the active metal sites instead of the actual linkers (1,4-benzenedicarboxylic acid). The defective UiO-66 with higher porosity shows promising results with regards to catalytic activity and gas uptake.[18,19] More investigations must be carried out to determine the effect of missing-linker defects on the stability of MOFs.

UiO-66 is well known for its high thermal stability of up to 500 °C and its catalytic applications.[20] During thermal treatment, UiO-66 decomposes to zirconia, which is a MOF derivative.[21]

Although a considerable amount of research into the various aspects of stability as well as modifications of UiO-66 has been performed, its pattern of decomposition under various gaseous conditions has not yet been fully explored.[22] The focus of the present study is to determine the decomposition patterns of UiO-66 with missing-linker defects under oxidative, reductive and inert conditions. Highly defective MOFs have high BET surface areas and thus provide a better opportunity for use as active catalysts. The defective sites in the MOFs generated by the missing linkers or clusters can be filled with active catalytic species to obtain active MOFs useful for various catalytic applications. MOFs on thermal decomposition produce porous

---

[a] *Laboratory for Catalysis and Sustainable Chemistry, Paul Scherrer Institut, 5232 Villigen-PSI, Villigen, Switzerland. E-mail: jeroen.vanbokhoven@chem.ethz.ch; marco.ranocchiari@psi.ch*

[b] *Institute for Chemical and Bioengineering, ETH Zurich, Vladimir Prelog Weg 1, 8093 Zurich, Switzerland*

† Electronic supplementary information (ESI) available. See DOI: 10.1039/d1ra05411b

catalysts in the form of metal/metal oxides or their composites supported with a carbon matrix. By controlling the gaseous environment, the MOF derivatives can be designed accordingly. This study provides important information regarding MOF degradation in gaseous environments, which can be utilized to establish mechanistic approaches towards MOF degradation.

Experimental

Zirconium tetrachloride ($ZrCl_4$) was purchased from Merck, while benzene-1,4-dicarboxylic acid (H_2BDC), acetic acid and dimethylformamide (DMF) were purchased from Sigma Aldrich. These chemicals were used as received without further purification.

$ZrCl_4$ (1.17 g, 5.03 mmol) and H_2BDC (0.83 g, 5.00 mmol) were dissolved in DMF (40 mL). Acetic acid (8.4 mL) and water (0.54 mL) were added to the mixture, which was stirred at room temperature for 15 minutes in an ultrasonic bath. The resulting cloudy white suspension was divided into four 20 mL crimp vials and placed in a Biotage Initiator microwave reactor at a temperature of 120 °C for 15 minutes under constant stirring and at 1 bar pressure. After the reaction, the vials were air cooled and the white product was isolated by centrifugation at 7000 rpm for 15 minutes. The product was then soaked in DMF for four days, washed with acetone and soaked in acetone for one day. Finally, the product was washed with acetone and dried under vacuum in an oven at 75 °C for 16 hours.

In situ powder X-ray diffraction (PXRD) was carried out on a Bruker D8 Advance diffractometer at Bragg–Brentano geometry with a temperature increase from 100 °C to 600 °C in steps of 50 °C. The XRD patterns were collected in a 2θ range of $4°$ to $70°$ using a Cu Kα radiation of $\lambda = 1.5406$ Å and a LYNXEYE XE detector. The operating voltage and the current of the X-ray tube were 40 kV and 40 mA, respectively.

The Brunauer–Emmett–Teller (BET) surface area of the samples was determined by measuring the nitrogen sorption isotherms at 77 K on a Micromeritics Tristar II analyzer. The samples were activated under vacuum at 120 °C for 24 hours before starting the adsorption measurements.

Transmission electron microscopy (TEM) was performed on a Tecnai F30 (FEI, USA) microscope operated at 300 kV (field emission gun; Super Twin lens with a point resolution of *ca.* 2 Å). The images were recorded with a 4k camera using binning 2. The samples were dispersed in isopropanol and some drops of the suspension were placed onto copper TEM grids (lacey carbon, 300 mesh).

Thermogravimetric analysis (TGA) was performed on a Netzsch STA 449-F5 instrument coupled to an Aëolos QMS 403 D mass spectrometer. The samples were heated to 600 °C at a heating rate of 10 °C per minute in three gaseous environments: oxidative, reductive and inert. Al_2O_3 crucibles were used for the measurements.

Results and discussion

A highly defective UiO-66 sample with a BET surface area of 1827 $m^2\ g^{-1}$ was analyzed for its thermal and crystalline stability in different gaseous environments: oxidative (25% oxygen in nitrogen (PXRD)/argon (TG-MS)), reductive (8% hydrogen in nitrogen (PXRD)/argon (TG-MS)) and inert (nitrogen (PXRD)/argon (TG-MS)). The produced MOF

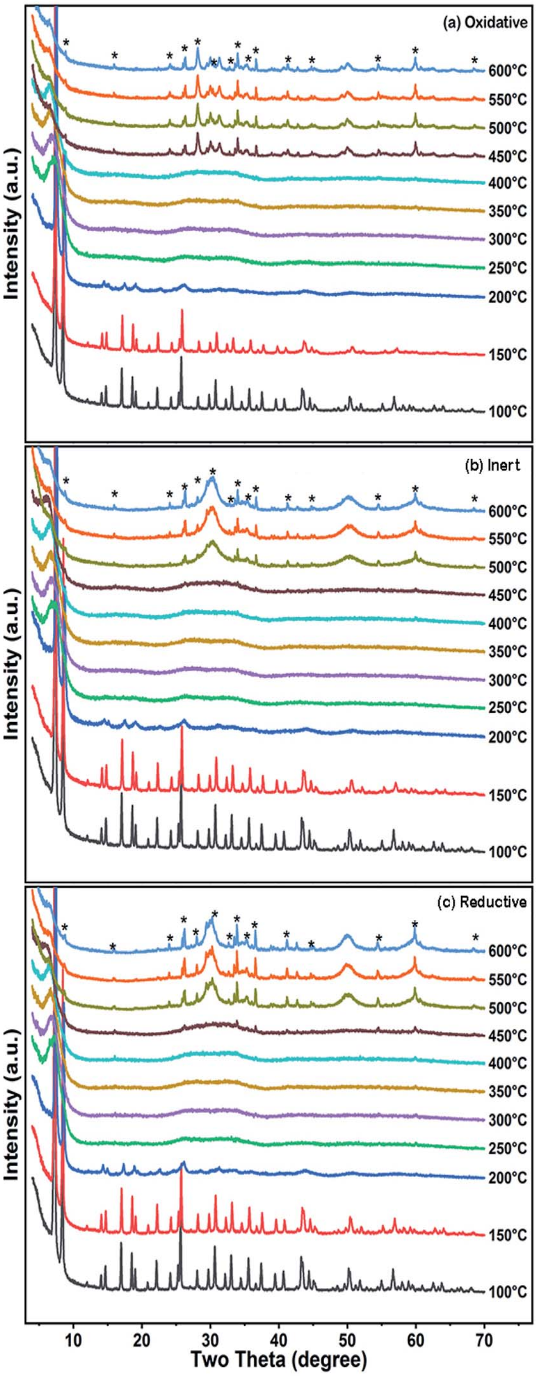

Fig. 1 *In situ* PXRD patterns of UiO-66 on heating from room temperature to 600 °C in an (a) oxidative, (b) inert and (c) reductive environment. The crystal structure of the MOF collapses below 250 °C, whereas the formation of crystalline zirconia takes place at 500 °C in the inert and reductive environments; in comparison to the oxidative environment, where it occurs at 450 °C. Above 450 °C, the highlighted peaks are due to the sample holder.

derivatives were further characterized by XRD and electron microscopy. *In situ* PXRD patterns were obtained at temperatures ranging from 100 °C to 600 °C (Fig. 1). The UiO-66 sample lost its crystalline framework at a very low temperature, *i.e.* below 250 °C, and remained amorphous up to 450 °C in the oxidative environment and up to 500 °C in the reductive and inert environments when new peaks started to arise due to the formation of zirconia. The final product obtained at 600 °C is predominantly tetragonal zirconia, which is embedded in the porous carbon support under the reductive and inert conditions. The PXRD pattern of the MOF material was measured after cooling the decomposed material, which remained amorphous showing that the loss of crystallinity was irreversible.

Fig. 2 shows the thermogravimetric analysis coupled with mass spectrometry (TG-MS) of the UiO-66 sample in three different atmospheres. It shows the first loss of mass at around 150 °C, which is due to the removal of water from the pores. At 230 °C, there was another slight loss of water due to the dehydroxylation of the zirconium cluster.[23] Further loss of mass

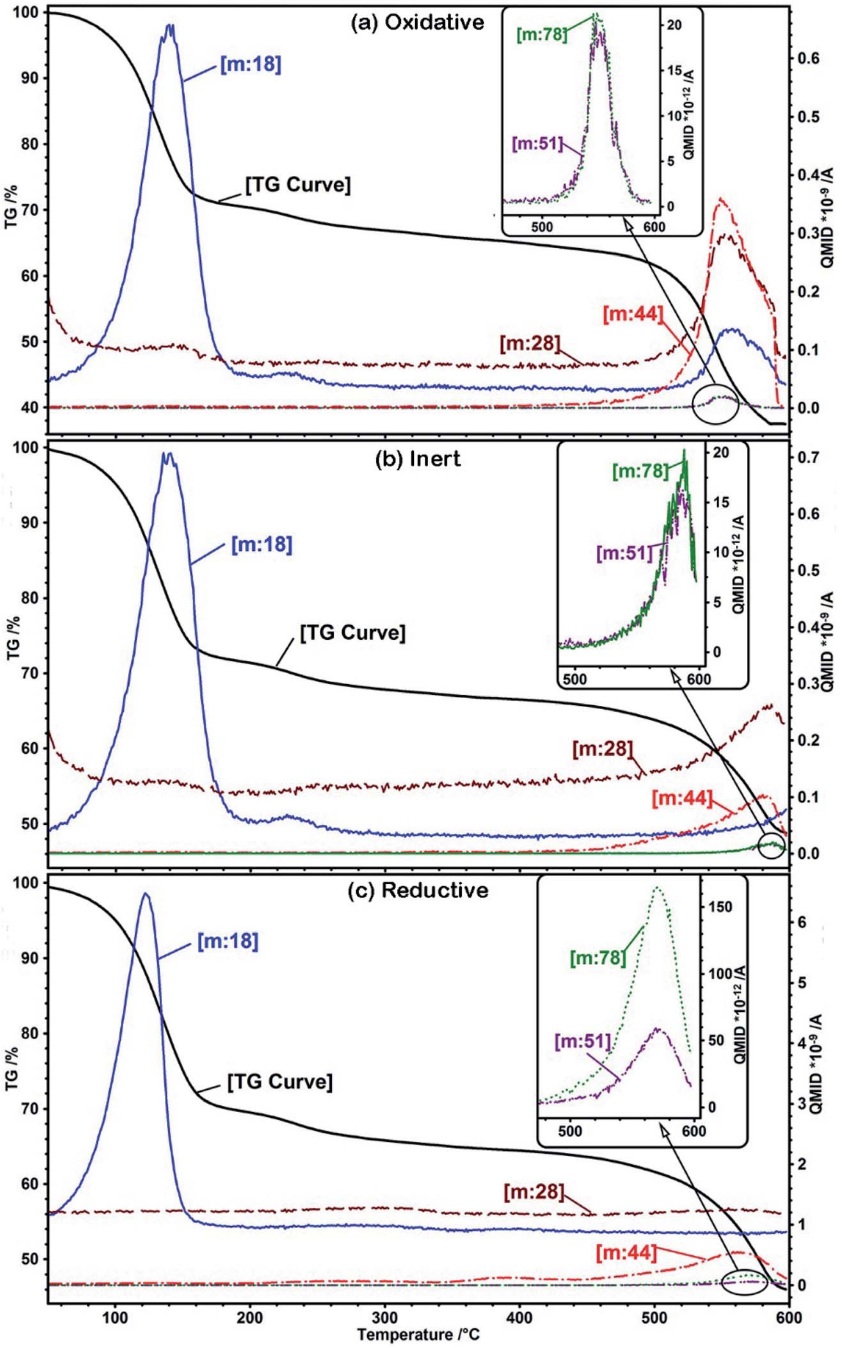

Fig. 2 TG-MS of UiO-66 under (a) oxidative (b) inert and (c) reductive conditions. The MOF decomposes at 450 °C in (a), whereas in (b) and (c) it decomposes at 500 °C.

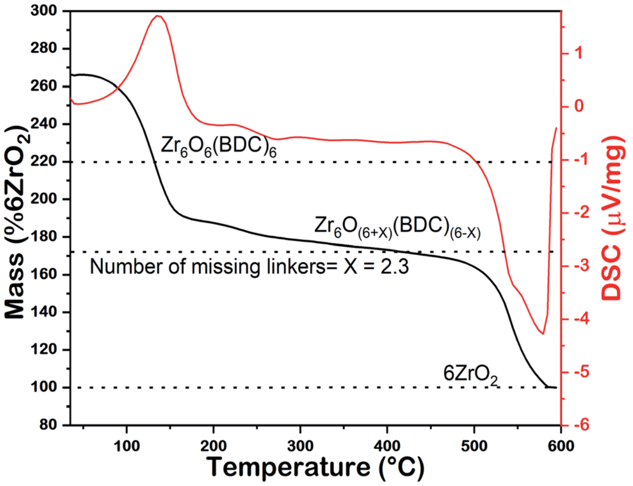

Fig. 3 Calculation of the number of missing BDC linkers per hexa-zirconium node. The final mass of $6ZrO_2$ is taken as 100 and that of the dehydroxylated perfect MOF before thermal decomposition is taken as 220.

occurs due to the degradation of the MOF, which starts at 450 °C in the oxidative atmosphere and at 500 °C in the inert and reductive atmospheres. MS monitoring shows that the major decomposition products are carbon dioxide and water along with some traces of benzene under oxidative conditions. Under inert and reductive conditions, the amount of carbon dioxide formed is very small and may have been generated by the decomposition of the carboxylates. The final mass of the products after TG under oxidative conditions is 38%, which is due to the formation of white-colored zirconia as the end product, whereas the masses of the final end products under the reductive and inert conditions are 46% and 48%, respectively, indicating the presence of black/grey unburnt carbon along with zirconia. It is evident that the presence of oxygen triggers the combustion of the MOF and it starts to decompose at a lower temperature than under inert conditions.

The high BET surface area of UiO-66 mainly depends on the defects in the MOFs, which can be introduced by various synthetic strategies.[20] A quantitative measurement of the defects has been done by calculating the number of missing BDC linkers per hexa-zirconium node from the TGA data according to the reported method[20] as shown in Fig. 3. In the TGA curve of the MOF sample taken from the oxidative environment, the final mass of the product ($6ZrO_2$) is taken as 100. The mass of the dehydroxylated MOF, $Zr_6O_6(BDC)_6$, corresponds to 220 (2.2 times the mass of $6ZrO_2$). The actual mass of UiO-66 before its thermal decomposition is compared with these values to calculate the number of missing linkers per hexa-zirconium node. For our sample, this number is 2.3, which is in agreement with its high BET surface area.

The nitrogen adsorption–desorption isotherms are shown in Fig. 4. The BET surface area of the original MOF sample was 1827 $m^2 g^{-1}$. The BET surface area measurements after heating under oxidative, reductive and inert conditions were recorded on another UiO-66 sample having a BET surface area comparable to the original one. The new MOF sample was heated ex-situ under inert, reductive and oxidative conditions up to 450 °C, at which the PXRD peaks disappeared. The BET surface

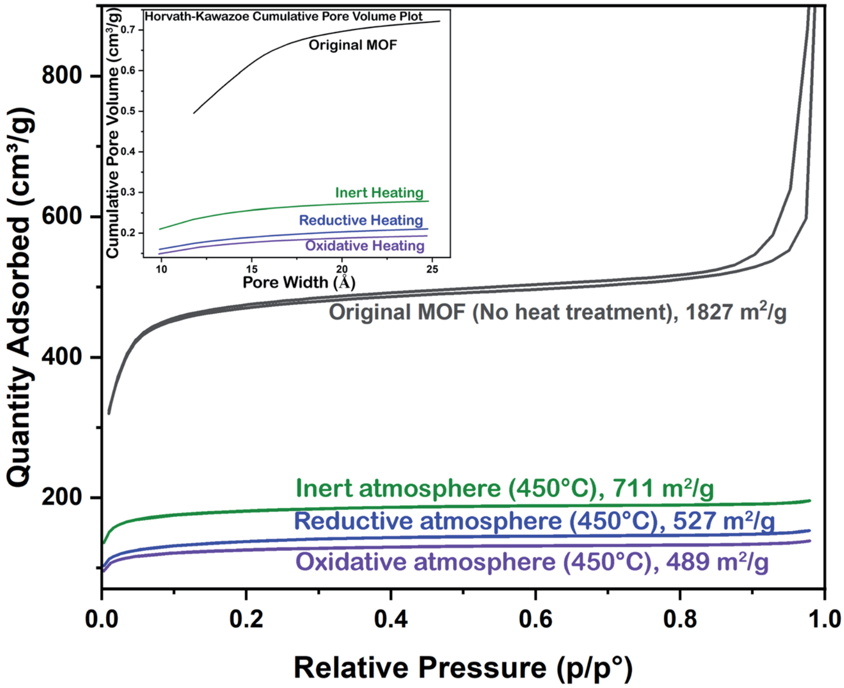

Fig. 4 Nitrogen adsorption–desorption isotherms of the UiO-66 samples without heating and after heating at temperatures where the crystalline framework collapses under different gaseous environments. Gaseous environment, heating temperature and the BET surface area are mentioned against each isotherm. Inset shows the H–K cumulative pore size plots of these samples.

Table 1 Maintenance of porosity after heating UiO-66 under different conditions

Heating condition	BET surface area ($m^2\ g^{-1}$)	*t*-Plot micropore area ($m^2\ g^{-1}$)	H–K maximum pore volume ($cm^3\ g^{-1}$)/relative pressure	Median pore width (Å)
No heating	1827	1452	0.722/0.167	11.79
Inert (450 °C)	711	600	0.278/0.161	9.89
Reductive (450 °C)	527	402	0.211/0.160	9.89
Oxidative (450 °C)	489	401	0.193/0.160	9.85

areas of the samples heated under inert, reductive and oxidative conditions are 711, 527 and 489 $m^2\ g^{-1}$, respectively. These results indicate that the nature of the gas has a great influence on porosity reduction while heating, with oxidative conditions being more drastic towards porosity reduction.

The Horvath–Kawazoe (H–K) cumulative pore volumes of all the samples were extracted from the nitrogen adsorption–desorption isotherms and are shown as the inset of Fig. 4. This shows the microporous behavior of all the samples. The H–K maximum pore volumes of the samples decrease as the BET surface area decreases, depending on the heat treatment of the MOF samples. The t-plot micropore area also shows a decreasing trend similar to the H–K pore size distribution. The data of the nitrogen sorption analysis are listed in Table 1. The retention of the BET surface area (711 $m^2\ g^{-1}$ under inert conditions, for example) indicates that after the fracture of the crystalline framework, there is a strong bond between the inorganic metal clusters (cations) and the organic linkers (anions).

Fig. 5 shows the TEM images of UiO-66, taken before and after heat treatment. The material, although decomposed, seems to preserve the original morphology, even after heating to 600 °C under reductive and inert conditions, while it is lost under oxidative conditions. This is because all the carbon atoms

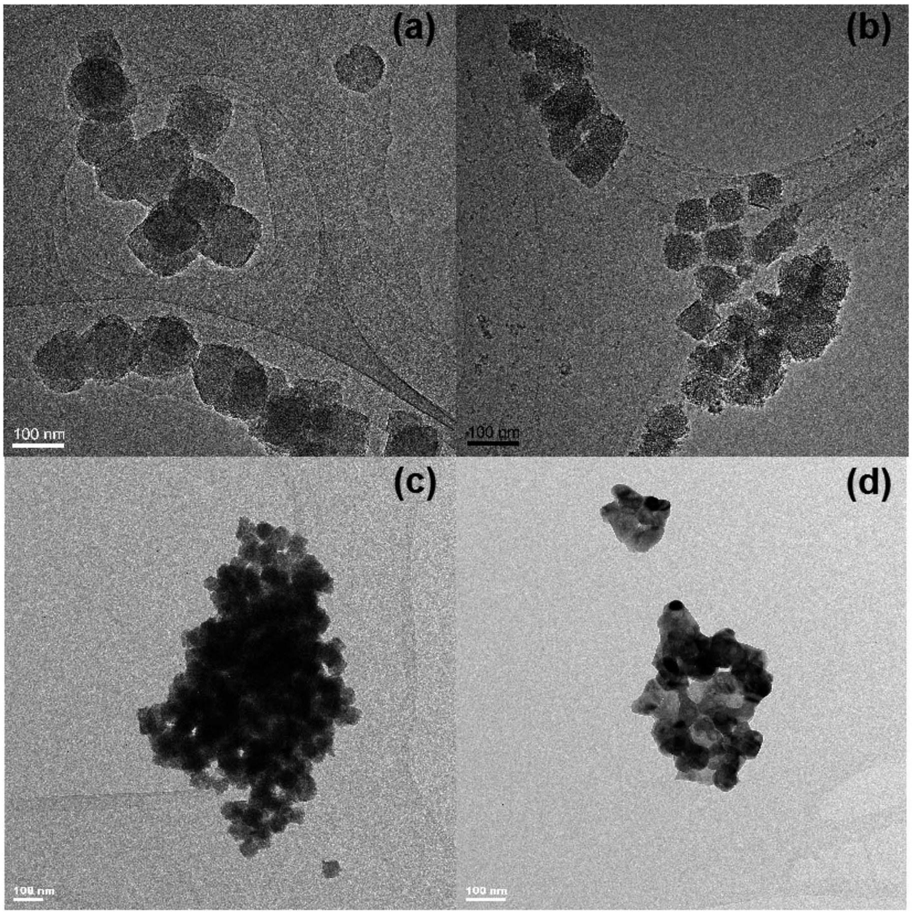

Fig. 5 TEM images of UiO-66 particles (a) before heating; and (b)–(d) after heating to 600 °C under reductive, inert and oxidative conditions, respectively.

of the ligands are combusted to carbon dioxide, leaving only zirconia nanoparticles, which is clear from the TEM image of zirconia in Fig. 5(d). Under inert and reductive conditions, a majority of the carbon atoms of the ligands retain their initial positions and provide a porous matrix on which zirconia particles are embedded.

This work presents an interesting, never before reported breakdown phenomenon of the UiO-66 crystalline framework below 250 °C. This extraordinary phenomenon may be due to the highly defective nature of the MOF. The as-synthesized UiO-66 has a surface area of 1827 $m^2\ g^{-1}$, which is 1.5 times greater than that of the original defect-free UiO-66. The missing-linker defects in the crystalline framework provide an easy target for breakdown upon heating. Shearer *et al.*[20] reported another such example of framework breakdown at a lower temperature and claimed that UiO-66 synthesized at 100 °C at a BDC : Zr ratio of 2 : 1 (without modulator) lost crystallinity at 300 °C when heated in air for 12 hours, while another sample, which was synthesized at 220 °C, retained crystallinity up to 400 °C. In the former case, the sample had more defects and a surface area of 1340 $m^2\ g^{-1}$ compared to the sample in the latter case, which had a surface area of 1105 $m^2\ g^{-1}$. Furthermore, a comparison of the degradation pattern of UiO-66 in different gaseous environments provides a better understanding of the degradation process. The presence of oxygen facilitates degradation and all the organic matter is converted to carbon dioxide and water, whereas under inert conditions, the degradation process is relatively delayed, leaving a carbon matrix for the zirconia particles. The ordered arrangement of the zirconia particles over the carbon matrix indicates its potential for catalytic applications. The degradation behavior of UiO-66 in reductive gas is similar to that in inert gas. This shows that the MOF (the zirconia clusters) is quite stable with regards to reduction with hydrogen up to 600 °C.

Conclusions

Defect-rich UiO-66 with a high surface area shows that crystallinity is lost below 250 °C, although it is thermally stable up to 500 °C. The BET surface area of the MOF is affected variably when heated under different gaseous conditions. Heating under inert condition saves more porosity (711 $m^2\ g^{-1}$) as compared to that under reductive (527 $m^2\ g^{-1}$) or oxidative (489 $m^2\ g^{-1}$) conditions. The metal and ligands remain bonded after losing crystallinity over a wide range of temperature until thermal decomposition starts. The effect of a gaseous atmosphere also plays a prominent role in the thermally induced decomposition. In the reductive and inert atmospheres, the original morphology of the MOF crystal is preserved after the complete thermal decomposition of the MOF at 600 °C because the final product zirconia is supported by the carbon matrix of the organic part of the MOF.

Conflicts of interest

There are no conflicts to declare.

Acknowledgements

The authors acknowledge the contributions of Frank Kurmeich and Hannes Frey in obtaining the transmission electron microscopic images and SNF for providing financial support for this project at PSI.

References

1 A. E. Baumann, D. A. Burns, B. Liu and V. S. Thoi, *Commun. Chem.*, 2019, **2**, 86.
2 B. Wang, L.-H. Xie, X. Wang, X.-M. Liu, J. Li and J.-R. Li, *Green Energy Environ.*, 2018, **3**, 191–228.
3 H. Furukawa, K. E. Cordova, M. O'Keeffe and O. M. Yaghi, *Science*, 2013, **341**, 1230444.
4 H. C. Zhou, J. R. Long and O. M. Yaghi, *Chem. Rev.*, 2012, **112**, 673–674.
5 S. Devautour-Vinot, G. Maurin, C. Serre, P. Horcajada, D. Paula da Cunha, V. Guillerm, E. de Souza Costa, F. Taulelle and C. Martineau, *Chem. Mater.*, 2012, **24**, 2168–2177.
6 H. L. Wang, H. Yeh, Y. C. Chen, Y. C. Lai, C. Y. Lin, K. Y. Lu, R. M. Ho, B. H. Li, C. H. Lin and D. H. Tsai, *ACS Appl. Mater. Interfaces*, 2018, **10**, 9332–9341.
7 C. Healy, K. M. Patil, B. H. Wilson, L. Hermanspahn, N. C. Harvey-Reid, B. I. Howard, C. Kleinjan, J. Kolien, F. Payet, S. G. Telfer, P. E. Kruger and T. D. Bennett, *Coord. Chem. Rev.*, 2020, **419**, 213388.
8 M. Bosch, M. Zhang and H.-C. Zhou, *Adv. Chem.*, 2014, **2014**, 182327.
9 M. Ding, X. Cai and H.-L. Jiang, *Chem. Sci.*, 2019, **10**, 10209–10230.
10 R. Ricco, C. Pfeiffer, K. Sumida, C. J. Sumby, P. Falcaro, S. Furukawa, N. R. Champness and C. J. Doonan, *CrystEngComm*, 2016, **18**, 6532–6542.
11 S. Han, Y. Huang, T. Watanabe, S. Nair, K. S. Walton, D. S. Sholl and J. Carson Meredith, *Microporous Mesoporous Mater.*, 2013, **173**, 86–91.
12 A. J. Howarth, Y. Liu, P. Li, Z. Li, T. C. Wang, J. T. Hupp and O. K. Farha, *Nat. Rev. Mater.*, 2016, **1**, 15018.
13 A. J. Rieth, A. M. Wright and M. Dincă, *Nat. Rev. Mater.*, 2019, **4**, 708–725.
14 J. Ren, M. Ledwaba, N. M. Musyoka, H. W. Langmi, M. Mathe, S. Liao and W. Pang, *Coord. Chem. Rev.*, 2017, **349**, 169–197.
15 J. H. Cavka, S. Jakobsen, U. Olsbye, N. Guillou, C. Lamberti, S. Bordiga and K. P. Lillerud, *J. Am. Chem. Soc.*, 2008, **130**, 13850–13851.
16 M. R. DeStefano, T. Islamoglu, S. J. Garibay, J. T. Hupp and O. K. Farha, *Chem. Mater.*, 2017, **29**, 1357–1361.
17 L. Valenzano, B. Civalleri, S. Chavan, S. Bordiga, M. H. Nilsen, S. Jakobsen, K. P. Lillerud and C. Lamberti, *Chem. Mater.*, 2011, **23**, 1700–1718.
18 X. Feng, J. Hajek, H. S. Jena, G. Wang, S. K. P. Veerapandian, R. Morent, N. De Geyter, K. Leyssens, A. E. J. Hoffman, V. Meynen, C. Marquez, D. E. De Vos, V. Van Speybroeck,

K. Leus and P. Van Der Voort, *J. Am. Chem. Soc.*, 2020, **142**, 3174–3183.

19 C. A. Clark, K. N. Heck, C. D. Powell and M. S. Wong, *ACS Sustainable Chem. Eng.*, 2019, **7**, 6619–6628.

20 G. C. Shearer, S. Chavan, J. Ethiraj, J. G. Vitillo, S. Svelle, U. Olsbye, C. Lamberti, S. Bordiga and K. P. Lillerud, *Chem. Mater.*, 2014, **26**, 4068–4071.

21 M. H. Yap, K. L. Fow and G. Z. Chen, *Green Energy Environ.*, 2017, **2**, 218–245.

22 N. C. Burtch, H. Jasuja and K. S. Walton, *Chem. Rev.*, 2014, **114**, 10575–10612.

23 G. C. Shearer, S. Forselv, S. Chavan, S. Bordiga, K. Mathisen, M. Bjørgen, S. Svelle and K. P. Lillerud, *Top. Catal.*, 2013, **56**, 770–782.